24

AUTOMATED 3D ANALYSIS OF LARGE BRAIN MRI DATABASES

ALAN C. EVANS

In recent years, the study of gross neuroanatomy and its relationship to behavior and brain function has been reenergized by the advent of imaging techniques and the powerful computational tools with which to analyze high-resolution three-dimensional (3D) brain images (10,11,22,52,53). However, such high technology tools often demand that scientific questions be restated and made more amenable to quantitative analysis. Questions such as "How much normal variation is there in the size, shape, or location of an individual brain structure?" or "To what extent does functional architecture of the cortex depend on the anatomic boundaries between anatomic regions?" carry with them the assumption that the borders of individual structures can be specified accurately in any brain. In the past, basic questions of functional neuroanatomy were difficult to address in a systematic way in the living brain. We have learned much from anecdotal reporting of individual patients with various forms of brain lesion or from direct cortical stimulation during brain surgery, but the generalization of individual observation to the wider population has been confounded by the normal variation in brain structure itself. There is then a fundamental interest in understanding the nature of anatomic variability in the population, both for its relationship to functional variability and for the potential of using structural abnormality as a measure of development, normal aging, and disease. For instance, in some degenerative diseases like Huntington's disease and Alzheimer's disease, the sulci become more open and the ventricles become enlarged. Magnetic resonance imaging (MRI)-based measurements of these changes can lead to early diagnosis and treatment, but we need to understand the variation among normal brains first.

Although the study of postmortem neuroanatomy is a long-established science, the ability to accumulate the numbers of brains necessary to make statistically meaningful conclusions about cerebral anatomy is a relatively recent phenomenon. It is still difficult to identify reliably in any single brain the anatomic landmarks, boundaries, and other delimiting features necessary for any subsequent analysis. Thus, we face a new problem posed by this newfound technology and its inflexible demand that anatomic questions be posed in numerical rather than descriptive terms. The tools exist to image large numbers of brains noninvasively with MRI, but we are still struggling with how to extract the anatomic measurements necessary to answer the questions posed above. It is relatively easy to identify the precentral gyrus, but few researchers attempt to define its "top" and "bottom." Where does the inferior frontal sulcus end? Traditional brain atlases identify brain regions only by pointing to the middle of the region or surface feature, leaving the interfaces between regions unspecified. Neuroanatomists debate the exact boundary of even relatively simple structures such as the thalamus or caudate nucleus. With this context, new initiatives at various laboratories are attempting to standardize and codify the partitioning of the human brain into named regions, not without controversy. Traditional neuroanatomists debate among themselves about what parcellation scheme and nomenclature to use. Computer scientists argue among themselves about whether to use hierarchical, relational, object-oriented, or some other form of database structure to organize the brain parcellation. Both groups tend to misunderstand the importance of the other's concerns. Neurobiologists or physicians are not used to thinking in terms of inclusive sets where, for instance, every structure at one level is wholly included within a higher level organization, where all 3D pixels, i.e., voxels, within the brain space *must* be labeled as one of the structures in the partitioning scheme, or that the cerebrospinal fluid (CSF) ventricular spaces may be declared as being outside of "brain." Computer scientists tend to ignore the realities that many cortical sulcal features do not exist in every brain, and may be fragmented or have multiple occurrences. Some sophisticated analytic approaches for quantifying anatomic variability assume that a particular landmark can be perfectly identified in any brain when the reality is that errors of 5 to 10 mm typically occur, an error that is about

Alan C. Evans: Department of Neurology, McGill University, Montreal Neurological Institute, Montreal, Quebec, Canada.

the same magnitude as the true spatial variation being sought.

Despite heroic efforts in the recent past (2,29,58,60,62, 75,79,80), manual labeling of many individual MRI data sets in 3D is a labor-intensive effort that is not likely to be widely adopted. Fully automated techniques that produce accurate neuroanatomic segmentation in large numbers of MRI data sets are essential if questions of normal cross-sectional variability, normal longitudinal development, and detection of abnormality in single subjects or in groups are to be answered definitively. Many groups are now engaged in the field of MRI-based quantitative neuroanatomy, and an exhaustive review of the field is beyond the scope of this chapter. A representative sampling of activity by other groups in the field, categorized into the four forms of segmentation discussed in the subsequent Methods section, include the following:

- Tissue classification/voxel morphometry: This refers to MRI intensity-based classification of images into tissue classes and voxel-based statistical analysis of the resulting class maps. In normal brain, the tissue classes are typically gray matter, white matter, and CSF, although there is no reason in principle to restrict to these three tissue types. In these approaches, one or more co-registered MRI images of the same neuroanatomy, obtained using different acquisition protocols [e.g., T1-weighted, T2-weighted, proton density (PD), magnetization transfer), provide the input data. At each voxel the MRI intensity for each of the *N* input images provides an *N*-dimensional "feature vector." Ideally, each tissue class is identified by a unique feature vector. In practice, many confounding factors (e.g., tissue heterogeneity, MRI field distortions, partial volume effects, and image noise) blur the feature space and render it difficult to distinguish accurately even three tissue classes. Many different multivariate statistical methods exist to optimize the class labeling and, for most of them, more independent images (features) help to disentangle overlapping class distributions in feature space.

  Mapping the segmented images into stereotaxic space (69,70) allows for group analysis across a population of 3D data sets from different individuals. All of the machinery of random field statistical analysis developed for functional imaging then becomes available for structural analysis (1,5,30,31,35,54,56,57,81–83).
- Regional parcellation/atlas deformation: Delineation of brain regions within each tissue class (e.g., caudate nucleus in the gray matter class) is not possible using only the information available in the MR image(s) since there is not sufficient differentiation among these regions within the feature space. Some form of prior information on neuroanatomic boundaries is needed, usually in the form of a computerized brain atlas, to assist in 3D brain regional labeling. Regions can be identified by vector boundaries or by labeling of all internal voxels. The atlas or parcellation scheme can be used as a guide to manual segmentation or as the basis for automated regional segmentation in which the atlas space is deformed to match each new 3D brain image. The atlas template is matched to the new MRI volume through a variety of nonlinear deformation techniques, the most successful of which use image similarity criteria to deform one image into another.

  Once delineated in their native space it is possible to map the regional labels into stereotaxic space in much the same way as tissue class maps and to conduct voxel morphometry among groups using the random field statistical analysis (3,4,6,12,18,18,21,26,32,34,36,39–41,50,68).
- Surface extraction/cortical unfolding: Regional parcellation is generally quite successful at labeling relatively well-defined 3D brain regions, such as the thalamus, but is typically less successful in identifying cortical gyri. Indeed, the cortex as such is sufficiently important to merit special analytic treatment. Techniques have been developed to "extract" the exterior cortical surface automatically by boundary detection of the intensity interface between gray matter and subarachnoid CSF. To overcome partial effects, some groups have targeted the internal cortical margin at the interface between gray and white matter. Obtaining a measure of the two surfaces simultaneously allows for a measure of cortical thickness at each location over the cortical surface.

  Extraction of the cortical surface has prompted some groups to explore the potential of an "unfolded" cortical surface as a means of studying functional neuroanatomy on a two-dimensional (2D) plane. Arguably, this device reduces the variability of functional areas introduced by cortical folding in three dimensions. The mapping from 3D to 2D is a nontrivial task with many issues surrounding the optimal mapping function, with direct analogies to the well-known cartographic dilemmas of preservation of area, direction, distance etc. (7,8,20,27,28,38,49,55, 77,78).
- Sulcal extraction/analysis: The cortical sulci have held a historical position of prominence in functional neuroanatomy, in part because of their utility as approximate landmarks to functional areas. Recent interest has centered upon extracting not just the surface trace of the sulcus as a line but rather the depth of the sulcus as a ribbon. The latter approach provides more information on buried cortex and sulcal shape than a simple line trace, which can be related to genetic and developmental considerations (46,51,59,65,76).

In the United States, the Human Brain Project has specifically set out to foster the application of computational techniques, hardware, and algorithms to neuroscience at all spatial scales. We are involved in one of these applications operating at the gross morphology level. The International Consortium for Brain Mapping (ICBM) (52), seeks to create a so-called probabilistic human brain atlas (see below).

This chapter provides an overview of the methods developed by the Brain Imaging Centre (BIC) at the Montreal Neurological Institute for fully automated 3D segmentation of the ICBM database and other MRI databases like it, such as those collected for the creation of normal pediatric development and for evaluation of new pharmaceuticals. A key concept underlying this work is that of the analysis "pipeline," which takes 3D MRI volumes from large numbers of subjects and generates 3D statistical maps of adult brain morphology with no manual intervention. The pipeline concept has also been implemented for clinical trial analysis of MRI data from multiple sites. All data sets, across patients, time points, and pulse sequences, are mapped into a standardized 3D coordinate space for automatic segmentation and statistical analysis.

Once the MRI image has been segmented, each voxel in the 3D image space carries an anatomic label and a measure of the confidence in that label. This information can be used in a variety of ways to detect subtle neuroanatomic or neuropathologic changes:

- Single subject vs. group data for detection subtle of structural abnormality (e.g., misshapen corpus callosum)
- Intergroup cross-sectional comparison (e.g., Alzheimer's disease group vs. normal age-matched controls)
- Longitudinal study in a single subject (e.g., tumor growth, progressive atrophy)
- Longitudinal study in a group [e.g., early development and aging in normal populations, multiple sclerosis (MS) disease progression].

Illustrative example applications of some of these capabilities are described at the end of the chapter.

IMAGE SEGMENTATION METHODS

Within the BIC image analysis pipeline, MRI data are processed using a series of tools that provide measurements of volume, shape, size, and tissue composition of selected brain regions. These are summarized below. To manage the flow of MRI data through the pipeline, we have developed PCS (Production Control System), which allows the rapid implementation and parallel execution of analysis pipelines for processing large MRI databases. Each processing stage in the pipeline is performed by a single command. PCS allows the user to specify this command with its options, input and output files, and dependencies on other stages in the pipeline using a simple script language. Efficient coarse-grain parallelism is achieved by distributing the individual jobs over a network of workstations. PCS monitors the status of each job and submits a new job when the prerequisites for submission have been satisfied (typically the completion of all stages on whose output data the stage depends). The major elements of this environment include (Fig. 24.1):

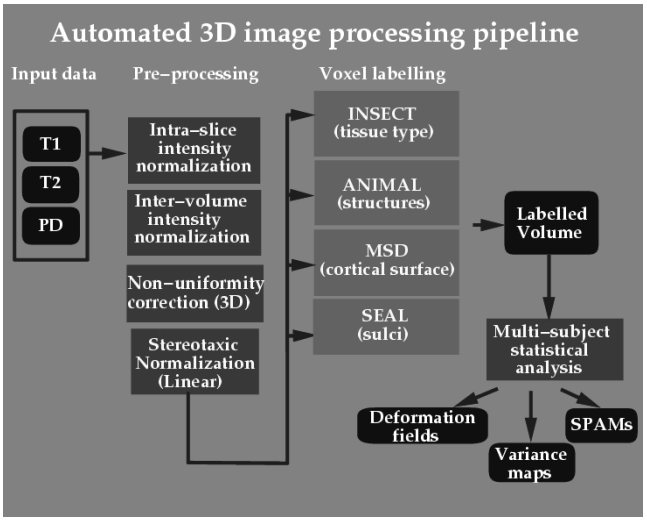

FIGURE 24.1. Brain Imaging Centre (BIC) pipeline environment for magnetic resonance imaging (MRI) processing: major components of pipeline analysis of large ensembles of MRI multispectral data sets. Each multispectral data set yields labeled maps of tissue type, three-dimensional (3D) brain region, and cortical topology.

- Thin-slice MRI data acquisition (typically 1-mm axial sampling, with 1-mm isotropic voxels).
- Multimodal, multidimensional stereotaxic data format (MINC).
- MRI simulator for validation of segmentation algorithms (MRISIM).
- Correction for coil-dependent 3D intensity nonuniformities (N3).
- Within-subject registration of different sequence volumes (MINCTRACC).
- Cross-subject mapping into a standardized "stereotaxic" 3D coordinate space (MRITOTAL).
- Fully automated 3D classification of gray/white/CSF tissue classes (INSECT).
- Fully automated 3D regional segmentation based on prior atlas templates (ANIMAL).
- Fully automated 3D extraction of gray/CSF and gray/white cortical interfaces (MSD, ASP).
- Computer-assisted 3D labeling of individual sulci (SEAL).

Stereotaxic Image Format—MINC

A fundamental aspect of this pipeline environment and its interaction with other sites within ICBM is the MINC image format for intersite data communication. MINC (Medical Image Net CDF), developed at the MNI by Peter Neelin, is a multidimensional, multimodality image file format that supports stereotaxic coordinate representation.

Image volumes can be explored in real time in 3D with continuous update of stereotaxic coordinates. Image files with different native voxel dimensions can be compared directly without regard for the original acquisition sampling grid. This simplifies stereotaxic analysis of MRI data ensembles collected with different voxel dimensions.

MRI Simulation—MRISIM

To assist in the evaluation of these segmentation tools, we created an average MRI data set of a single young normal male, by repeated MRI scanning followed by linear alignment of all volumes. A total of 27 separate MRI scans were collected. The improved signal-to-noise ratio (SNR) in the composite MRI, termed ICBM27, produces a high-definition data set (37), suitable for brain atlas construction, validation of segmentation/mapping algorithms, and MRI simulation. (Note: Since it incorporates the structural idiosyncracies of a single brain, it is not intended for use as a high-definition master data set for stereotaxic normalization.) This data set has been segmented manually to create an accurate digital phantom (17) for use as the source template of an MRI simulator, MRISIM (43).

MRISIM requires as input a set of "fuzzy" structure maps, one for each distinct tissue (or structure) type to be modeled, in which each voxel value is the probability of that voxel containing that tissue (structure) type. Such maps are generated by algorithms like INSECT or ANIMAL (see below) applied to a high-SNR data set. The MRI signal is simulated by solving the Bloch equations for the specified pulse sequence and tissue relaxation characteristics. Noise is modeled from first principles rather than by adding some parametric (e.g., gaussian) noise distribution to the expectation image (42). MRISIM has been used in validation studies for correction of MRI intensity nonuniformity (67) and tissue classification (84). It has been used to create a database of 108 simulate MRI images [3 slice thicknesses $\times$ 3 tissue contrasts (T1/T2/PD) $\times$ 3 noise levels $\times$ 4 levels of radiofrequency (RF) inhomogeneity], available at Web site *http://www.bic.mni.mcgill.ca*.

Correction for 3D Intensity Nonuniformity—N3

A major problem for automated MRI image segmentation is the slowly varying change in signal intensity over the image, caused principally by nonuniformities in the radiofrequency field (Fig. 24.2). Apparent signal from any one tissue type is therefore different from one brain area to another, confusing automated segmentation algorithms that assume constant signal for one tissue type. We have developed a fully automated 3D technique for inhomogeneity correction, modeling inhomogeneity as the convolution of the true MRI intensity histogram with a blurring kernel. This effective kernel can be estimated and deconvolved by iterative entropy maximization. The method is applicable to any pulse sequence, field strength, and scanner (66,67).

Intrasubject Image Alignment—MINCTRACC

Alignment of images from the same subject, either from the same modality at different times in a longitudinal study or from different modalities, is achieved using a linear version of ANIMAL (see below), constrained to a six-parameter (three rotation, three translation) rigid-body transformation (15).

Stereotaxic Transformation—MRITOTAL

Stereotaxic transformation is achieved using a simple nine-parameter linear [three rotation, three translation, three scale, (15)] transformation to match the image volume to a master data set already resident in stereotaxic space. The master data set therefore defines the gross dimensions and orientation of stereotaxic space. We have previously con-

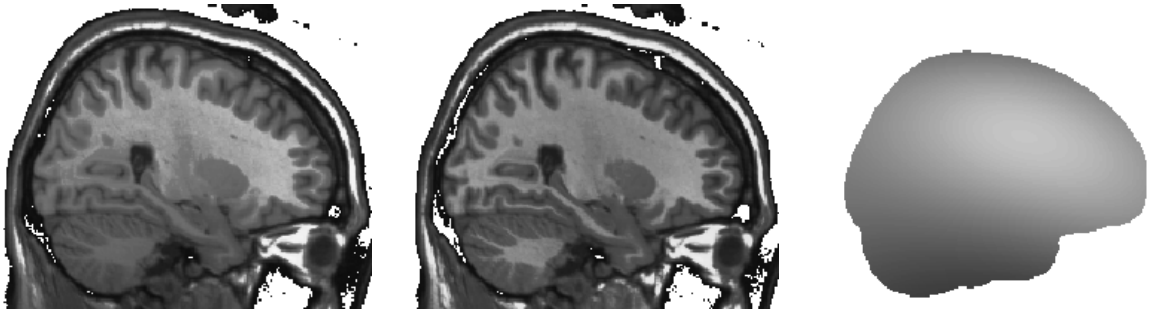

FIGURE 24.2. N3 correction for intensity nonuniformity. MRI image before (*left*) and after (*middle*) correction for nonuniformity field (*right*), estimated using N3. Note the increased uniformity of white matter regions.

structed a composite stereotaxic MRI data set drawn from 305 normal subjects, sampled on a 1-mm voxel grid (24), as that master data set. This mean data set, now termed ICBM305, has been circulated to over 100 international sites and defines the stereotaxic space for the SPM statistical package. That data set was derived from T1-weighted data with 2-mm-thick slice data. More recently, this has been superseded by a composite data set derived from 1-mm-thick data collected within the ICBM project (see below). That latter data set, while exhibiting higher contrast and more anatomic detail than the original ICBM305, was nevertheless mapped into the space of the ICBM305 using the nine-parameter MRITOTAL and is therefore a derivative of that first data set.

Tissue Classification—INSECT

We have developed an algorithm for tissue classification, known as INSECT (Intensity-Normalized Stereotaxic Environment for Classification of Tissue) (25,63,84). The algorithm operates upon multispectral (typically T1-, T2-, PD-weighted) data sets. In a series of preprocessing steps, each MRI data set is corrected for intensity nonuniformity (67), interslice normalization, and intersubject intensity normalization (Fig. 24.3). Stereotaxic transformation is then performed (15). An artificial neural network (ANN) classifier with one hidden layer is used to assign each voxel to a tissue type (gray/white/CSF) based on its MRI intensity feature space. The algorithm also employs tissue likelihood, based on the spatial location of the voxel in stereotaxic space, as orthogonal prior information to constrain the feature-space assignment. For example, periorbital fat exhibits a similar feature-space signal as white matter and, without consideration of spatial location, would be classified as white matter. Spatial masks expressing the normal distribution of tissue classes in the population (see Fig. 24.8) indicate that the likelihood of finding white matter in the periorbital stereotaxic region is small, and reduce the likelihood of misclassifi-

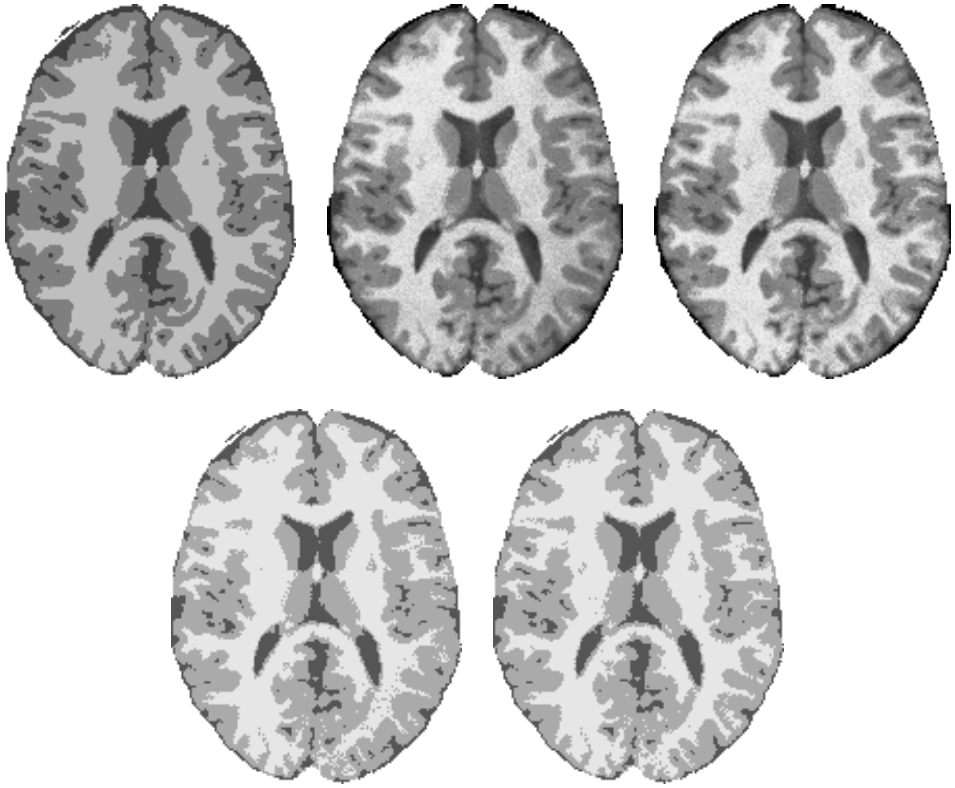

FIGURE 24.3. Classification with and without correction for intensity nonuniformity: tissue classification with INSECT with and without correction for nonuniformity using N3. An idealized 3D digital phantom was created from by segmentation of a high–signal-to-noise ratio (SNR) data set (17, 37). The initial phantom data (*top left*) contains three classes: cerebrospinal fluid (CSF) (*black*), gray matter (*dark gray*), and white matter (*light gray*). This phantom was used to generate a simulated MRI image with (*top middle*) and without (*top right*) a 20% inhomogeneity running from *top left* to *bottom right* of the image. The INSECT-classified image without prior N3 correction (*bottom left*) exhibits artifactually thicker cortex at *bottom right* and thinner cortex at *top left* of the image, respectively, a consequence of the field inhomogeneity gradient. This artifact is removed in the N3-corrected classification (*bottom right*).

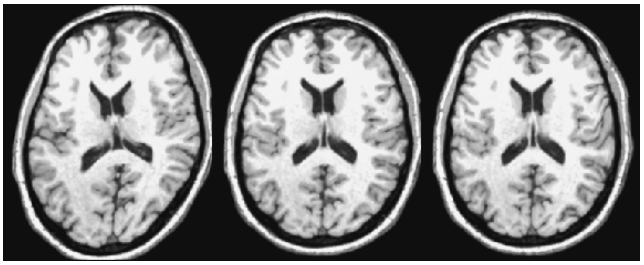

FIGURE 24.4. ANIMAL warping. Slice through a 3D ANIMAL deformation. The *left* image was warped to match the *right*, with the result in the *middle*.

ation. INSECT operates on an arbitrary number of input images and generates a user-selected number of output tissue maps.

Regional Parcellation—ANIMAL

Manual labeling of brain voxels is both time-consuming and subjective. We have previously developed an automated algorithm to perform this labeling in 3D (13). The ANIMAL algorithm (Automated Nonlinear Image Matching and Anatomical Labeling), deforms one MRI volume to match another, previously labeled, MRI volume. It builds up the 3D nonlinear deformation field in a piecewise linear fashion, fitting cubical neighborhoods in sequence using a mutual information residual for parameter optimization (Fig. 24.4). The algorithm is applied iteratively in a multiscale hierarchy. At each step, image volumes are convolved with a 3D gaussian blurring kernel of successively smaller width [32-, 16-, 8-, 4-, and 2-mm full-width at half-maximum (FWHM)]. Anatomic labels are defined in the new volume by interpolation from the original labels, via the spatial mapping of the 3D deformation field. Originally, ANIMAL used 3D gradient magnitude as the image property to be matched. The ridge-tracking Lvv operator is now used to extract additional topologic information on brain shape in each image. Furthermore, the surface trace of major sulci, represented as 3D line segments, can be used as local constraints on image deformation (14,16). Both steps increase the correspondence of cortical anatomy across brains.

Cortical Surface Segmentation and Unfolding—ASP

We have previously developed a fully automated procedure for unfolding the entire human cortex, using an algorithm that automatically fits a 3D mesh model to the cortical surface extracted from MRI (47). This algorithm, MSD, uses an iterative minimization of a cost function that balances the distance of the deforming surface from (a) the target surface, and (b) the previous iteration surface (Fig. 24.5). Specification of the relative weight of these competing forces allows MSD to range from unconstrained (data-driven) deformation to tightly constrained (model-preserving) deformation. Further shape-preserving constraints to penalize excessive local stretching and bending of the model surface are also employed. The initial mesh surface can be chosen arbitrarily to be a simple geometric object, such as a sphere, an ellipsoid, or two independently fitted hemispheres. The MSD algorithm has formed the basis of cortical analysis at both MNI and UCLA within the ICBM project (71–73). Recently, the algorithm has been extended to allow multiple concentric surfaces to be mapped simultaneously. The new algorithm, Automatic Segmentation

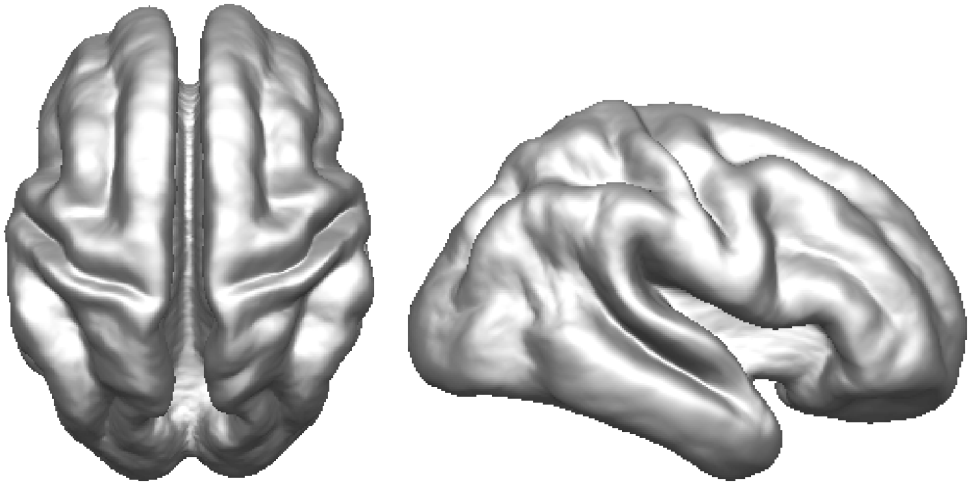

FIGURE 24.5. Average cortical surface. Average of 150 normal cortical surfaces. Note the prominence of the major gyral and sulcal features common to all brains.

using Proximities (ASP), has the following refinements and capabilities (48), compared with the earlier MSD version:

- A boundary search along the normal local surface is used to increase the range of attraction of edges.
- The use of proximity constraints with appropriate weights excludes the potential for impossible self-intersecting surface configurations.
- Some arbitrary weights are replaced by more intuitive geometric constraints.
- Multiple surfaces, models, and data sets may be combined into a single objective function.
- Automatic identification of the total cerebral cortical surface from MR images is achieved in a robust way with respect to partial volume effects.
- A preliminary map of cortical gray matter thickness has been produced and related to previous studies.
- A higher resolution average brain surface has been created using the deeper sulcal penetration of ASP compared to earlier versions of this algorithm (47).

As an alternative form of stereotaxy applicable to cortical analysis, ASP also provides a fully automated mapping from 3D to an unfolded surface space. Since ASP iteratively deforms a starting 3D polygonal mesh onto the 3D cortical surface, the inverse mapping projects this fitted surface and topologic feature at each surface vertex back to the model space (47,48). Individual anatomic features such as gyral ridges and sulcal valleys are converted to measures of topology, e.g., curvature, mapped on to the model surface. These can be analyzed in terms of 2D variability on the surface of the starting model using a 2D surface coordinate space (Fig. 24.6).

Sulcal Extraction and Labeling—SEAL

We have implemented an automated sulcal extraction and labeling algorithm (SEAL) (45). At every voxel on the ASP-generated exterior cortical isosurface, SEAL calculates the two principal curvatures: k1, the mean curvature, and k2, the gaussian curvature (g = k1 * k2). Voxels with negative

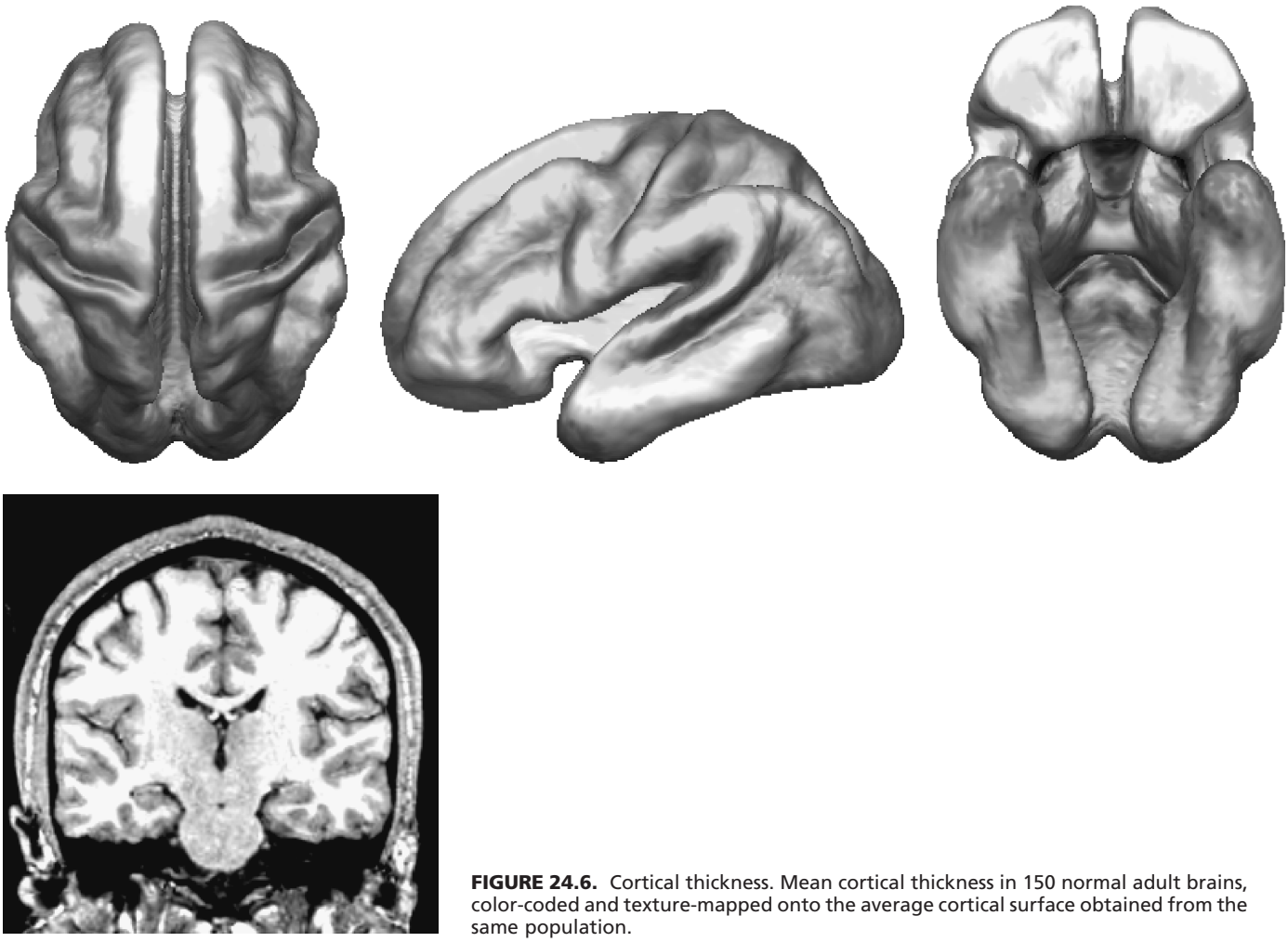

FIGURE 24.6. Cortical thickness. Mean cortical thickness in 150 normal adult brains, color-coded and texture-mapped onto the average cortical surface obtained from the same population.

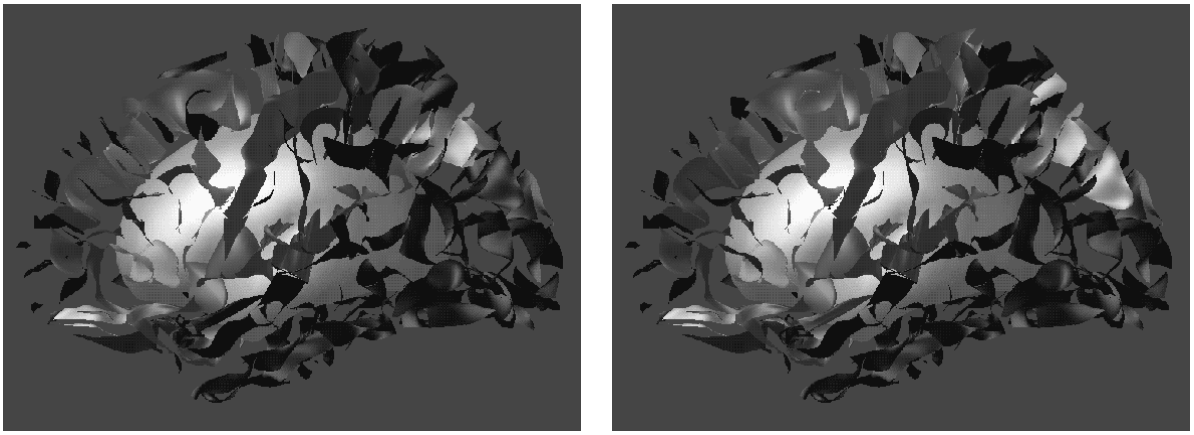

FIGURE 24.7. Use of spatial priors for automatic sulcus labeling within the sulcal extraction and labeling algorithm (SEAL). 3D representation of labeled sulcal folds occurs either automatically with SEAL, using prior probabilities (*left*), or manually labeled by a neuroanatomist (*right*). Different colors represent different sulcal labels, e.g., central sulcus is colored magenta (the smooth object is an average MRI surface, reduced in scale, included only to provide context for the sulcal maps). The automated and manual labeling of the sulci are in broad agreement, although some differences are apparent.

mean curvature, belonging to sulci, are extracted and pruned to obtain a set of sulcal traces on the cortical surface. SEAL extracts the buried sulcus with an ''active ribbon'' that evolves in 3D from a superficial trace to the bottom of a sulcus by optimizing an energy function. We have defined a relational graph structure that stores, for each sulcus, its length, depth, and orientation, as well as attributes, e.g., hemisphere, lobe, sulcus type, connecting sulci, etc. Sulcal labeling is performed semiautomatically by tagging a sulcal trace in the 3D graph and selecting from a menu of candidate labels. The menu is restricted to most likely candidates by the use of sulcal probabilistic maps. SEAL identifies the sulci maps that overlap with each selected sulcus with highest likelihood (44,45) (Fig. 24.7).

SAMPLE APPLICATIONS

ICBM: Multicenter Consortium on Statistical Neuroanatomy

The International Consortium for Brain Mapping (ICBM) multicenter initiative was launched in 1993 as part of the Human Brain Project (52). Its overall goal is to create a 3D probabilistic brain atlas, based on MRI volumes from 450 normal adult brains. Within the ICBM project, all scans at all sites were collected with a strictly defined protocol, specifying three MRI volumes per subject (a 1-mm-thick, 1-mm-spaced gradient echo sequence for T1-weighted data and a 2-mm-thick, 1-mm-spaced double-echo sequence for PD and T2-weighted volumes). This database as been segmented using the pipeline environment described above and the variability captured in the form of probability maps as follows. Neuroanatomic variability can be conveniently represented in the form of 3D stereotaxic maps where each voxel expresses the likelihood of finding a particular structure at that location. By labeling one structure, e.g., caudate nucleus, in an ensemble of stereotaxic MRI volumes, a continuous 3D probability field for that structure (0% to 100% at each voxel), termed a statistical probability anatomy map (SPAM), can be constructed and used to test for group difference, e.g., pediatric versus adult brains, or outliers. For visualization purposes, these statistical maps can the thresholded at any level of structural probability to create probability isosurfaces suitable for surface-rendering and 3D display. Example SPAMs are shown for (a) gray/white/CSF tissue classes (INSECT, Fig. 24.8); (b) all major cortical gyri, cerebellum, and deep nuclei (ANIMAL, Figs. 24.8 and 24.9); and (c) cortical surface (ASP) (23).

Multicenter Clinical Trial Image Analysis

The principles of pipeline analysis described above for large databases of normal brain MRI data are equally applicable for population analysis of neuropathology or for tracking structural change over time, such as the progressive tissue atrophy, which occurs in some degenerative diseases. Indeed, the MRI analysis employed within the ICBM project was originally developed for a multicenter phase III clinical trial of a new pharmaceutical for treatment of multiple sclerosis. In this trial, 14 centers in the U.S. and Canada collected a total of 1,850 data sets, each data set composed of T1, T2, and PD volumes, from 514 subjects. All data collection was coordinated by the BIC clinical trials group, which performed quality control before trial launch and for all data shipped to the BIC for processing. Pipeline analysis of the database was used to generate 3D statistical maps of normal tissues and of MS lesions. In validation studies, the

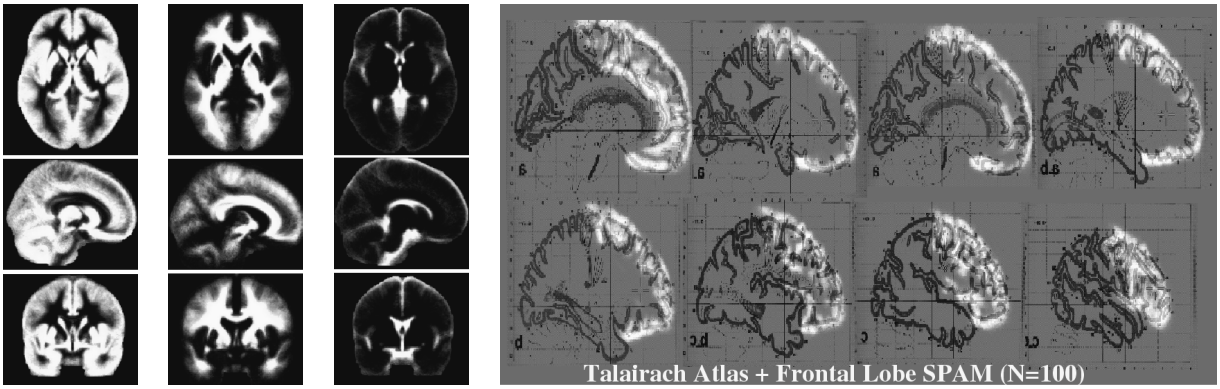

FIGURE 24.8. Tissue probability maps. **Left**: Cuts through INSECT-generated 3D tissue class maps for gray matter, white matter, and cerebrospinal fluid (CSF). **Right**: Serial sagittal sections through Talairach atlas with ANIMAL-generated probabilistic frontal cortex SPAM (statistical probability anatomy map) overlaid. In both cases 100 subjects were used to generate the SPAMs.

results obtained with this automated approach for a subset of images were compared with those obtained by totally manual methods at seven established MRI/MS sites in Europe and North America. The results of the comparison indicated no significant differences between the BIC approach and the mean result obtained across the seven sites. They also indicate considerable variability among the sites themselves when analyzing the same data, which emphasizes the importance of the reproducibility of results obtained with a fully automated approach.

After correction for MRI intensity inhomogeneity, interslice and intervolume intensity normalization, and stereotaxic transformation, the multispectral data were tissue classified to identify MS lesion voxels for each patient time point. Figure 24.10 shows a 3D rendering of a probability map for lesion distribution obtained from all data sets. It shows the most likely locations for MS lesions within a population and is a convenient way to distill a large amount of population data into a single entity. Tests of drug effect are reduced to testing for a significant group difference in the overall volume of this distribution above a given threshold when partitioned into drug and placebo groups.

NIMH Intramural Pediatric Database

As part of an ongoing collaboration with Drs. Jay Giedd and Judy Rapoport at the National Institute of Mental Health (NIMH) Child Psychiatry Branch, the BIC image analysis pipeline has been used to process a large pediatric MRI database collected at the NIMH. Subjects were scanned on a General Electric 1.5 tesla Signa scanner using a 3D SPGR protocol. Approximately 1,800 T1-weighted images with slice thickness of 1.5 to 2.0 mm in the axial plane have

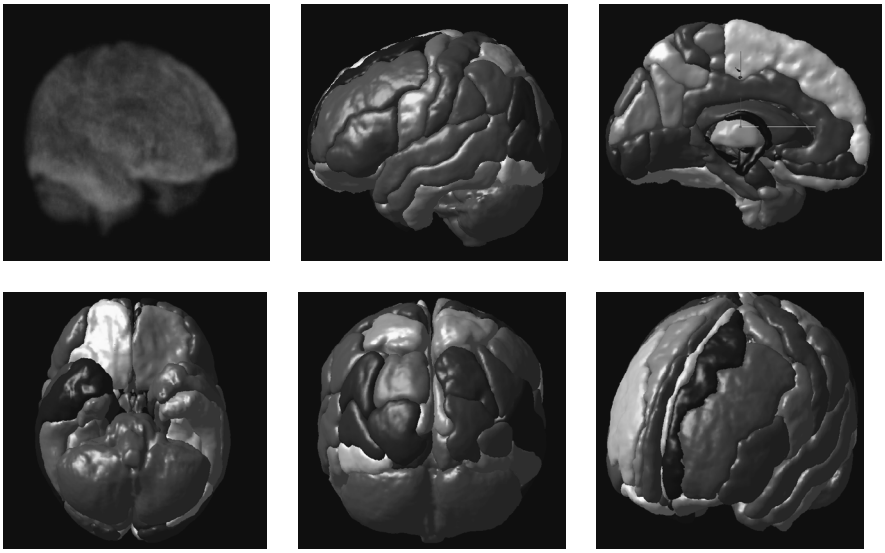

FIGURE 24.9. Rendered probabilistic atlas. Volume rendering (*top left*) and surface renderings (*all others*) of the 3D probabilistic atlas ($N = 100$). For the surface renderings, the SPAMs were thresholded at the 40% level to generate regional probability isosurfaces.

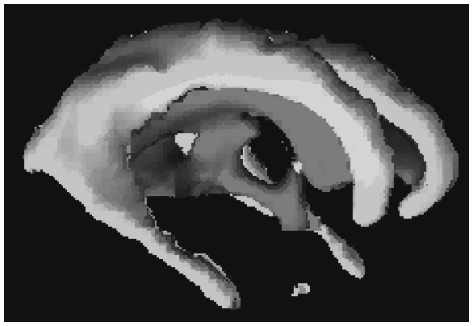

FIGURE 24.10. Multiple sclerosis (MS) lesion probability map. 3D renderings of probability maps for MS lesion (*light region*) and ventricle (*dark region*), obtained from 460 patients.

been obtained in approximately 600 children aged 3 to 18 from a number of subgroups:

- Normal development: A subset of this database, 111 normal children aged 4 to 17, was processed using the INSECT algorithm. All data were resampled into stereotaxic space using a simple nine-parameter linear transformation prior to image segmentation. Regression of population mean white matter intensity at each stereotaxic voxel against age yielded a regression map with significant correlation in the left arcuate fasciculus and the bilaterally in the internal capsule (33,61). The former tract links the anterior and posterior speech regions, while the latter is part of the corticospinal motor tract. These areas are continuously developing during maturation and it is tempting to interpret the results as increased myelination in these areas during development.

  A subset of the intramural NIMH database has also been analyzed by the ICBM group at UCLA under the direction of Arthur Toga (74). Using MSD-generated surfaces and tensor field analysis, they produced four-dimensional quantitative maps of growth patterns in the developing brain. Serial scanning in children aged 3 to 15 years across time spans of up to 4 years revealed a rostrocaudal wave of growth in the corpus callosum, a fiber system that relays information between brain hemispheres (Fig. 24.11). Peak growth rates, in fibers innervating association and language cortices, were attenuated after puberty, and contrasted sharply with a severe, spatially localized loss of subcortical gray matter. Conversely, at ages 3 to 6 years, the fastest growth rates occurred in frontal networks that regulate the planning of new actions.
- Child-onset schizophrenia: Fifteen patients with childhood-onset schizophrenia and 34 temporally yoked, healthy adolescents, scanned twice with an interval of 4 years, were analyzed using the pipeline (64). Lobar gray and white matter volumes were obtained with INSECT and ANIMAL. A significant decrease in cortical gray matter volume was seen for healthy controls in the frontal (2.6%) and parietal (4.1%) regions. For the childhood-onset schizophrenia group, there was a decrease in volume in these regions (10.9% and 8.5%, respectively) as well as a 7% decrease in volume in the temporal gray matter. Thus, the childhood-onset schizophrenia group showed a distinctive disease-specific pattern, with the frontal and temporal regions showing the greatest between-group differences. Changes in white matter volume did not differ significantly between the two groups. Patients with very early onset schizophrenia exhibit a fourfold greater decrease in cortical gray matter volume during adolescence and a disease-specific pattern of change.
- Attention-deficit/hyperactivity disorder (ADHD): Anatomic studies of boys with ADHD have previously detected volumetric differences in basal ganglia, prefrontal regions, and the cerebellar vermis. This study sought to

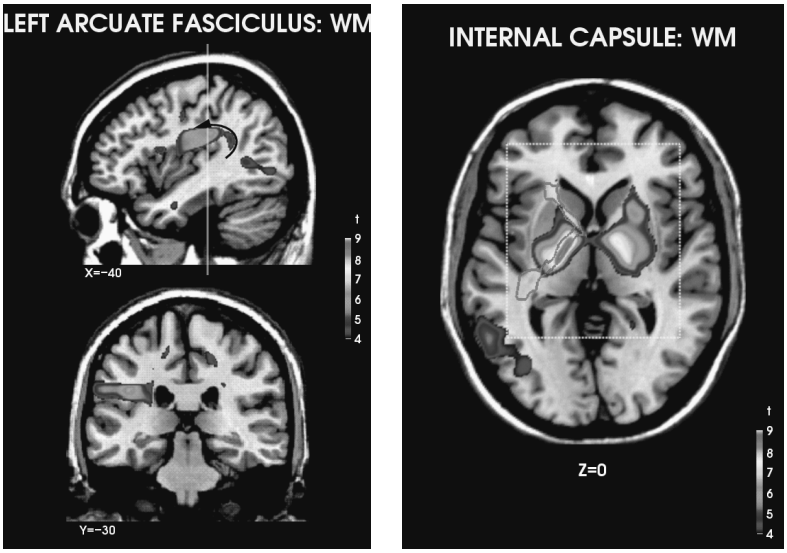

FIGURE 24.11. White matter density changes during pediatric development. Regression maps of white matter density changes over the age range from 4 to 17 (61). These maps show increased white matter density, possibly myelination, in the left arcuate fasciculus (*left*) and internal capsule (*right*), white matter tracts implicated in the development of language and motor skills, respectively.

replicate those findings in young girls. MRI data from 53 girls with ADHD and 44 healthy matched female controls, ages 5 to 15, were analyzed using ANIMAL. Significantly smaller volumes were observed in prefrontal brain regions, caudate nucleus, globus pallidus, and amygdala bilaterally. The posterior-inferior cerebellar vermis volume and the rostrum of the corpus callosum were also significantly smaller in the ADHD group. Significantly smaller volumes were seen in the same brain regions as previously reported in boys with ADHD. As in boys, ADHD in girls is associated with anatomic deviations in corticostriatal-pallidal-thalamic circuits and in the posterior-inferior cerebellar vermis (9).

NIH Extramural Pediatric MRI Database

The NIMH intramural database above has been acquired with only T1-weighted information and sparse behavioral information from a variety of subgroups, including approximately 200 normal children aged 3 to 8. While this database will provide much valuable information on pediatric development, there remains a need to create a more complete database of MRI information from a larger cohort of normal children, well-characterized by behavioral batteries. Therefore, a recent joint initiative by three National Institutes of Health (NIH) agencies (NIMH, NICHD, NINDS) has been launched to create such an MRI database of normal pediatric development in 550 children. This project, drawing upon a clinical trial model, will collect identical imaging and behavioral data at seven U.S. sites. The data will be consolidated into a single database at the BIC for pipeline analysis and eventual dissemination to the community. Each child in the age range of 5 to 18 will be scanned three times over a 6-year period. Behavioral batteries covering the major performance criteria will be collected at each time point. A younger cohort of approximately 100 children, aged 0 to 5, will undergo a more frequent scanning protocol and an age-appropriate behavioral battery. Magnetic resonance spectroscopy (MRS) and diffusion tensor imaging (DTI) information will also be collected at three of the sites to provide information on developmental neurochemistry, myelination, and fiber tract development.

SUMMARY AND FUTURE DIRECTIONS

This chapter has presented an overview and sample applications of the MRI analysis pipeline environment at the Brain Imaging Centre (BIC) of the Montreal Neurological Institute. The key conceptual elements of this environment are as follows:

1. The use of stereotaxic space for consolidation of large ensembles of MRI data into a common spatial frame for analysis of gross neuroanatomy;
2. Fully automated 3D image preprocessing and segmentation;
3. Statistical analysis using voxel-bases random field theory and general linear models;
4. Incorporation of nonimaging parameters such as behavioral variables, demographic information, and genetic data into the statistical models.

The pipeline is highly modular, allowing for separate development and continued upgrading of the individual elements making up the pipeline. Processing is distributed across the BIC computing infrastructure using the PCS control scripts to optimize the utilization of resources. It has application in a variety of settings from basic neuroscience through clinical research to clinical trials. However, the current environment is focused on gross morphology. Conventional MRI allows us to collect gross anatomic information from a large sample of brains and develop population statistics. Unfortunately, this level of analysis provides no information about the cellular and molecular organization of the brain at a finer scale. A full understanding of functional neuroanatomy links function to macroscopic anatomy via these ultrastructural segregations. High-field MRI offers new possibilities, providing resolution of a few hundred microns over limited volumes. Sectioning, staining, and optical digitization of cadaver brains allow even finer spatial and chemical resolution in limited numbers of brains. A number of sites are bringing together these new acquisition technologies with the concepts of 3D stereotaxic mapping to create probabilistic maps at this finer scale. The advantage of the stereotaxic approach is that information from these many techniques operating at different spatial scales can be consolidated over many years into a systematic description of the whole brain structure and function. Such a rich database of information on both cerebral structure and function, accessible to sophisticated computational and statistical exploration, offers exciting possibilities for future brain research and clinical practice. Quite apart from direct hypothesis testing, such an environment may allow for the detection of hitherto unsuspected patterns of interaction among normal brain elements and the isolation of constellations of measurements that characterize specific disease states.

REFERENCES

1. Abell F, Krams M, Ashburner J, et al. The neuroanatomy of autism: a voxel-based whole brain analysis of structural scans. *Neuroreport* 1999;10(8):1647–1651.
2. Adolphs R, Damasio H, Tranel D, et al. A role for somatosensory cortices in the visual recognition of emotion as revealed by three-dimensional lesion mapping. *J Neurosci* 2000;20(7):2683–2690.
3. Amunts K, Malikovic A, Mohlberg H, et al. Brodmann's areas 17 and 18 brought into stereotaxic space-where and how variable? *Neuroimage* 2000;11(1):66–84.
4. Ashburner J, Andersson JL, Friston KJ. High-dimensional image registration using symmetric priors. *Neuroimage* 1999;9(6 pt 1): 619–628.
5. Ashburner J, Friston KJ. Voxel-based morphometry-the methods. *Neuroimage* 2000;11(6 pt 1):805–821.
6. Ashburner J, Hutton C, Frackowiak R, et al. Identifying global

anatomical differences: deformation-based morphometry. *Hum Brain Mapping* 1998;6(5–6):348–357.
7. Bakircioglu M, Grenander U, Khaneja N, et al. Curve matching on brain surfaces using frenet distances. *Hum Brain Mapping* 1998;6(5–6):329–333.
8. Carman GJ, Drury HA, Van Essen DC. Computational methods for reconstructing and unfolding the cerebral cortex. *Cerebral Cortex* 1995;5(6):506–517.
9. Castellanos FX, Giedd JN, Berquin PC, et al. Quantitative brain magnetic resonance imaging in girls with attention-deficit/hyperactivity disorder. *Arch Gen Psychiatry* 2001;58:289–295.
10. Caviness VS Jr, Lange NT, Makris N, et al. MRI-based brain volumetrics: emergence of a developmental brain science. *Brain Dev* 1999;21(5):289–295.
11. Caviness VS Jr, Makris N, Lange NT, et al. Advanced applications of MRI in human brain science. *Keio J Med* 2000;49(2): 66–73.
12. Christensen GE, Joshi SC, Miller MI. Volumetric transformation of brain anatomy. *IEEE Trans Med Imaging* 1997;16(6): 864–877.
13. Collins DL, Holmes CJ, Peters TM, et al. Automatic 3D model-based neuroanatomical segmentation. *Hum Brain Mapping* 1995; 3:190–208.
14. Collins DL, LeGoualher G, Venegopal R, et al. Cortical constraints for non-linear cortical registration. In: *Proceedings of 4th International Conference on Visualization in Biomedical Computing VBC 1996*. 1996:307–316.
15. Collins DL, Neelin P, Peters TM, et al. Automatic 3D registration of MR volumetric data in standardized Talairach space. *J Comput Assist Tomogr* 1994;18(2):192–205.
16. Collins DL, LeGoualher G, Barillot C, et al. Cortical constraints in fully automated non-linear spatial normalization of 3d brain images. *IEEE Trans Med Imaging* 2000; *submitted*.
17. Collins DL, Zijdenbos AP, Kollokian V, et al. Design and construction of a realistic digital brain phantom. *IEEE Trans Med Imaging* 1998;17(3):463–468.
18. Crespo-Facorro B, Kim JJ, Andreasen NC, et al. Human frontal cortex: an MRI-based parcellation method. *Neuroimage* 1999; 10(5):500–519.
19. Csernansky JG, Joshi S, Wang L, et al. Hippocampal morphometry in schizophrenia by high dimensional brain mapping. *Proc Natl Acad Sci USA* 1998;95(19):11406–11411.
20. Dale AM, Fischl B, Sereno MI. Cortical surface-based analysis. I. segmentation and surface reconstruction. *Neuroimage* 1999; 9(2):179–194.
21. Dale AM, Sereno MI. Improved localization of cortical activity by combining EEG and MEG with MRI cortical surface reconstruction: a linear approach. *J Cogn Neurosci* 1993;5:162–176.
22. Duncan JS, Ayache N. Medical image analysis: progress over two decades and the challenges ahead. *IEEE Trans Pattern Analysis Machine Intelligence* 2000;22(1):85–106.
23. Evans AC, Collins DL, Holmes CJ, et al. A 3d probabilistic atlas of normal human neuroanatomy. Proceedings of the 3rd International Conference on Functional Mapping of Human Brain, 1997.
24. Evans AC, Collins DL, Mills SR, et al. 3D statistical neuroanatomical models from 305 MRI volumes. In: *IEEE Conference Record, Nuclear Science Symposium and Medical Imaging Conference*, San Francisco. 1993:1813–1817.
25. Evans AC, Frank JA, Antel J, et al. The role of MRI in clinical trials of multiple sclerosis: comparison of image processing techniques. *Ann Neurol* 1997;41:125–132.
26. Fiez JA, Damasio H, Grabowski TJ. Lesion segmentation and manual warping to a reference brain: intra- and interobserver reliability. *Hum Brain Mapping* 2000;9(4):192–211.
27. Fischl B, Sereno MI, Dale AM. Cortical surface-based analysis. II: Inflation, flattening, and a surface-based coordinate system. *Neuroimage* 1999;9(2):195–207.
28. Fischl B, Sereno MI, Tootell RB, et al. High-resolution intersubject averaging and a coordinate system for the cortical surface. *Hum Brain Mapping* 1999;8(4):272–284.
29. Frank RJ, Damasio H, Grabowski TJ. Brainvox: an interactive, multimodal visualization and analysis system for neuroanatomical imaging. *Neuroimage* 1997;5(1):13–30.
30. Friston KJ, Frith CD, Liddle PF, et al. Comparing functional (PET) images: the assessment of significant change. *J Cereb Blood Flow Metab* 1991;11:690–699.
31. Friston KJ, Holmes AP, Worsley KJ, et al. Statistical parametric maps in functional imaging: a general linear approach. *Hum Brain Mapping* 1995;2:189–210.
32. Gibaud B, Garlatti S, Barillot C, et al. Computerized brain atlases as decision support systems: a methodological approach. *Artif Intell Med* 1998;14(1–2):83–100.
33. Giedd JN, Blumenthal J, Jeffries NO, et al. Brain development during childhood and adolescence: A longitudinal MRI study. *Nature Neurosci* 1999;2(10):861–863.
34. Goldszal AF, Davatzikos C, Pham DL, et al. An image-processing system for qualitative and quantitative volumetric analysis of brain images. *J Comput Assist Tomogr* 1998;22(5):827–837.
35. Harris G, Andreasen NC, Cizadlo T, et al. Improving tissue classification in MRI: a three-dimensional multispectral discriminant analysis method with automated training class selection. *J Comput Assist Tomogr* 1999;23(1):144–154.
36. Hogan RE, Mark KE, Wang L, et al. Mesial temporal sclerosis and temporal lobe epilepsy: MR imaging deformation-based segmentation of the hippocampus in five patients. *Radiology* 2000; 216(1):291–297.
37. Holmes CJ, Hoge R, Collins DL, et al. Enhancement of MR images using registration for signal averaging. *J Comput Assist Tomogr* 1998;22(2):324–333.
38. Joshi M, Cui J, Doolittle K, et al. Brain segmentation and the generation of cortical surfaces. *Neuroimage* 1999;9(5):461–476.
39. Kennedy DN, Lange N, Makris N, et al. Gyri of the human neocortex: an MRI-based analysis of volume and variance. *Cerebral Cortex* 1998;8(4):372–384.
40. Kennedy DN, O'Craven KM, Ticho BS, et al. Structural and functional brain asymmetries in human situs inversus totalis. *Neurology* 1999;53(6):1260–1265.
41. Kim JJ, Crespo-Facorro B, Andreasen NC, et al. An MRI-based parcellation method for the temporal lobe. *Neuroimage* 2000; 11(4):271–288.
42. Kwan R, Evans AC, Pike GB. An extensible MRI simulator for post-processing evaluation. In: *Proceedings of the 4th International Conference on Visualization in Biomedical Computing, VBC 1996*. Hamburg: 1996:135–140.
43. Kwan RKS, Evans AC, Pike GB. MRI simulation-based evaluation of image processing and classification methods. *IEEE Trans Med Imaging* 1999;18(11):1085–1097.
44. LeGoualher G, Argenti AM, Duyme M, et al. Statistical sulcal shape comparisons: application to the detection of genetic encoding of the central sulcus shape. *Neuroimage* 2000;11(5): 564–574.
45. LeGoualher G, Procyk E, Collins DL, et al. Automated extraction and variability analysis of sulcal neuroanatomy. *IEEE Trans Med Imaging* 1999;18(3):206–217.
46. Lohmann G, von Cramon DY, Steinmetz H. Sulcal variability of twins. *Cerebral Cortex* 1999;9(7):754–763.
47. MacDonald D, Avis D, Evans AC. Multiple surface identification and matching in magnetic resonance imaging. Visualization in Biomedical Computing 1994. *Proc SPIE* 1994;2359:160–169.
48. MacDonald D, Kabani N, Avis D, et al. Automated 3d extraction of inner and outer surfaces of cerebral cortex from MRI. *Neuroimage* 2000;12(3):340–356.
49. Magnotta VA, Andreasen NC, Schultz SK, et al. Quantitative

in vivo measurement of gyrification in the human brain: changes associated with aging. *Cerebral Cortex* 1999;9(2):151–160.
50. Makris N, Meyer JW, Bates JF, et al. MRI-based topographic parcellation of human cerebral white matter and nuclei ii. rationale and applications with systematics of cerebral connectivity. *Neuroimage* 1999;9(1):18–45.
51. Manceaux-Demiau A, Bryan RN, Davatzikos C. A probabilistic ribbon model for shape analysis of the cerebral sulci: application to the central sulcus. *J Comput Assist Tomogr* 1998;22(6): 962–971.
52. Mazziotta JC, Toga AW, Evans AC, et al. A probabilistic atlas of the human brain: theory and rationale for its development. *Neuroimage* 1995;2:89–101.
53. Mazziotta JC, Toga AW, Evans AC, et al. Digital brain atlases [letter]. *Trends Neurosci* 1995;18(5):210–211.
54. Miller M, Banerjee A, Christensen G, et al. Statistical methods in computational anatomy. *Stat Methods Med Res* 1997;6(3): 267–299.
55. Montagnat J, Delingette H, Scapel N, et al. Surface simplex meshes for 3d medical image segmentation. Proceedings, ICRA millennium conference. IEEE International Conference on Robotics and Automation Symposia Proceedings (Cat. No. 00CH37065), IEEE, part vol. 1, 2000.
56. Mummery CJ, Patterson K, Price CJ, et al. A voxel-based morphometry study of semantic dementia: relationship between temporal lobe atrophy and semantic memory. *Ann Neurol* 2000; 47(1):36–45.
57. Nopoulos P, Flaum M, O'Leary D, et al. Sexual dimorphism in the human brain: evaluation of tissue volume, tissue composition and surface anatomy using magnetic resonance imaging. *Psychiatry Res* 2000;98(1):1–13.
58. Nopoulos P, Swayze V, Flaum M, et al. Incidence of ectopic gray matter in patients with schizophrenia and healthy control subjects studied with MRI. *J Neuropsychiatry Clin Neurosci* 1998; 10(3):351–353.
59. Ono M, Kubik S, Abernathey CD. *Atlas of cerebral sulci.* Stuttgart: Georg Thieme Verlag, 1990.
60. Paus T, Tomaiuolo F, Otaky N, et al. Human cingulate and paracingulate sulci: pattern, variability, asymmetry, and probabilistic map. *Cerebral Cortex* 1996;6:207–214.
61. Paus T, Zijdenbos A, Worsley K, et al. Structural maturation of neural pathway in children and adolescents. *Science* 1999;283: 1908–1911.
62. Penhune VB, Zatorre RJ, MacDonald JD, et al. Interhemispheric anatomical differences in human primary auditory cortex: probabilistic mapping and volume measurement from MR scans. *Cerebral Cortex* 1996;6(5):661–672.
63. Pruessner JC, Li LM, Serles W, et al. Volumetry of hippocampus and amygdala with high-resolution MRI and three-dimensional analysis software: minimizing the discrepancies between laboratories. *Cerebral Cortex* 2000;10(4):433–442.
64. Rapoport JL, Giedd JN, Blumenthal J, et al. Progressive cortical change during adolescence in childhood-onset schizophrenia: a longitudinal magnetic resonance imaging study. *Arch Gen Psychiatry* 1999;56(7):649–654.
65. Sastre-Janer FA, Regis J, Belin P, et al. Three-dimensional reconstruction of the human central sulcus reveals a morphological correlate of the hand area. *Cerebral Cortex* 1998;8(7):641–647.
66. Sled JG, Zijdenbos AP, Evans AC. A comparison of retrospective intensity nonuniformity correction methods for MRI. In: *Information processing in medical imaging.* 1997:459–464.
67. Sled JG, Zijdenbos AP, Evans AC. A non-parametric method for automatic correction of intensity non-uniformity in MRI data. *IEEE Trans Med Imaging* 1998;17(1):87–97.
68. Subsol G, Thirion JP, Ayache N. Application of an automatically built 3d morphometric brain atlas: study of cerebral ventricle shape. In: *Visualization in biomedical computing.* 4th International Conference, VBC 1996 Proceedings. Berlin: Springer-Verlag, 1996:373–382.
69. Talairach J, Szikla G, Tournoux P. *Atlas d'anatomie stereotaxique du telencephale.* Paris: Masson, 1967.
70. Talairach J, Tournoux P. *Co-planar stereotactic atlas of the human brain: 3-dimensional proportional system: an approach to cerebral imaging.* Stuttgart: Georg Thieme Verlag, 1988.
71. Thompson P, MacDonald D, Mega MS, et al. Quantifying and correcting for variable cortical morphology in functional imaging using a deformable probabilistic brain atlas. In: *Human brain mapping,* vol 4. 1997:5423.
72. Thompson PM, Schwartz C, Toga AW. High-resolution random mesh algorithms for creating a probabilistic 3d surface atlas of the human brain. *Neuroimage* 1996;3:19–34.
73. Thompson PM, Toga AW. A surface-based technique for warping three-dimensional images of the brain. *IEEE Trans Med Imaging* 1996;15(4):402–417.
74. Thompson PM, Giedd JN, Woods RP, et al. Growth patterns in the developing human brain detected using continuum-mechanical tensor maps. *Nature* 2000;404(6774):190–193.
75. Tibbo P, Nopoulos P, Arndt S, et al. Corpus callosum shape and size in male patients with schizophrenia [see comments]. *Biol Psychiatry* 1998;44(6):405–412.
76. Vaillant M, Davatzikos C. Finding parametric representations of the cortical sulci using an active contour model. *Med Image Anal* 1997;1(4):295–315.
77. Van Essen DC, Drury HA. Structural and functional analyses of human cerebral cortex using a surface-based atlas. *J Neurosci* 1997;17(18):7079–7102.
78. Van Essen DC, Drury HA, Joshi S, et al. Functional and structural mapping of human cerebral cortex: solutions are in the surfaces. *Proc Natl Acad Sci USA* 1998;95(3):788–795.
79. Wassink TH, Andreasen NC, Nopoulos P, et al. Cerebellar morphology as a predictor of symptom and psychosocial outcome in schizophrenia. *Biol Psychiatry* 1999;45(1):41–48.
80. Westbury C, Zatorre RJ, Evans AC. Quantifying variability in the planum temporale: a probability map. *Cerebral Cortex* 1999; 9:392–405.
81. Worsley KJ, Evans AC, Marrett S, et al. A three-dimensional statistical analysis for CBF activation studies in human brain. *J Cereb Blood Flow Metab* 1992;12:900–918.
82. Worsley KJ, Marrett S, Neelin P, et al. A unified statistical approach for determining significant signals in images of cerebral activation. *Human Brain Mapping* 1996;4(1):58–73.
83. Wright IC, McGuire PK, Poline J-B, et al. A voxel-based method for the statistical analysis of gray and white matter density applied to schizophrenia. *Neuroimage* 1995;2:244–252.
84. Zijdenbos AP, Evans AC, Riahi F, et al. Automatic quantification of multiple sclerosis lesion volume using stereotaxic space. In: *Proceedings of the 4th International Conference on Visualization in Biomedical Computing,* VBC 1996. 1996:439–448.